frontiers | Frontiers in Earth Science

TYPE Original Research
PUBLISHED 07 March 2024
DOI 10.3389/feart.2024.1373353

OPEN ACCESS

EDITED BY
Tianshou Ma,
Southwest Petroleum University, China

REVIEWED BY
Mengke An,
Hong Kong Polytechnic University, China
Hongwei Wang,
China University of Mining and Technology, China

*CORRESPONDENCE
Songfeng Guo,
guosongfeng@mail.iggcas.ac.cn

RECEIVED 19 January 2024
ACCEPTED 23 February 2024
PUBLISHED 07 March 2024

CITATION
Guo S, Li J, Qi S, Zheng B, Zhang Y, Zou Y, Zhu W, Waqar FM and Zada K (2024), Stress disturbance around Xianshuihe fault zone in the eastern Qinghai–Tibet Plateau and implication for fault stability.
Front. Earth Sci. 12:1373353.
doi: 10.3389/feart.2024.1373353

Stress disturbance around Xianshuihe fault zone in the eastern Qinghai–Tibet Plateau and implication for fault stability

Songfeng Guo[1,2,3]*, Jinxuan Li[1,4], Shengwen Qi[1,2,3], Bowen Zheng[1,2,3], Yaguo Zhang[4], Yu Zou[1,2,3], Weiwei Zhu[1,2,3], Faisal Muhammad Waqar[1,2,3] and Khan Zada[1,2,3]

[1]Key Laboratory of Shale Gas and Geoengineering, Institute of Geology and Geophysics, Chinese Academy of Sciences, Beijing, China, [2]Innovation Academy of Earth Science, Chinese Academy of Sciences, Beijing, China, [3]College of Earth and Planetary Sciences, University of Chinese Academy of Sciences, Beijing, China, [4]School of Civil Engineering, Chang'an University, Xi'an, China

The Xianshuihe fault zone in the eastern Qinghai–Tibetan Plateau is an important active tectonic boundary. Understanding its stress state is important for characterizing the dynamic evolution of the Qinghai–Tibet Plateau and the mechanism of the frequent occurrence of large earthquakes. Using 30 years of *in-situ* stress data from the Xianshuihe active fault zone, we statistically analyzed the spatial distribution characteristics of the stress in the region. The study area is generally characterized by a strike-slip stress field. Nevertheless, the stress state is vulnerable to topography and shows high spatial variation near the Earth's surface at a depth of 0–400 m. The local stress near the fault zone varies from the far-field stress. The orientations of the maximum horizontal principal stress possess an elliptical shape around the fault zone, while its magnitudes become hump-like as the distance increases from the fault. The large difference in properties between the fault zone and its adjacent rocks contributes to the differentiation of the direction of the local stress field near the fault. The results allow us to formulate a preliminary hypothesis that a rigid lateral extrusion model may control the nonuniformity of the local stress field in the Xianshuihe fault zone and preferentially interpret the tectonic uplift of the southeastern margin of the Qinghai–Tibet Plateau. Further, the stress accumulation in the shallow crustal regions of the Xianshuihe fault zone is relatively high, indicating that some segments of the fault zone are critically unstable. Kangding area (the Zheduotang segment and the Yalahe segment) and Luhuo segment hold relatively high potential for large earthquakes. The results of this study are of great significance for revealing the mechanism of fault–stress field interactions and for understanding the dynamic evolution mechanism of the uplift of the Qinghai–Tibet Plateau.

KEYWORDS

Xianshuihe fault zone, stress field, geomechanics, fault stability, Qinghai-Tibet Plateau

1 Introduction

Due to the collision of the Indian plate with the Eurasian plate, the Qinghai–Tibet Plateau (QTP) has been undergoing continuous uplift, resulting in horizontal tectonic movements and the deformation of the southeastern QTP Since the Miocene (Xu and Kamp, 2000; Shen et al., 2005; Royden et al., 2008). The Xianshuihe fault zone (XSHF), located in the junction zone of the Sichuan-Yunnan block and Baryan Har block in the southeastern QTP, is characterized by intense tectonic activity (Wang et a., 2014; Bai et al., 2018; Chevalier et al., 2018; Guo et al., 2018). This active intracontinental strike-slip fault plays a significant role in accommodating the post-collisional convergence between the Indian and Eurasian plates (Tapponnier and Molnar, 1977; Zhang G. et al., 2004). A number of strong earthquakes have been reported in the region since 1900 (Zhang et al., 2003; Zhang P. Z. et al., 2004), such as the Ms7.3 Daofu earthquake in 1923, the Ms7.5 Kangding earthquake in 1955, and the Ms7.6 Luhuo earthquake in 1973. Recently, the fault appears to be more active: two earthquakes occurred in 2022 and 2023 in Luding with magnitudes of Ms6.8 and Ms5.6, respectively. The mechanisms of earthquake clustering have attracted the attention of researchers for a long time, but have still not been fully understood.

Earthquake is a type of rock fracture driven by rock stress in the Earth's crust (Alexander, 1997; Oglesby and Day, 2002; Liao et al., 2003; Liu et al., 2008; Guo et al., 2009; Duan, 2010). Knowledge of the stress state of the Earth's crust is very important for understanding regional tectonics and predicting the stability of faults (Fleitout and Froidevaux, 1983; Zoback, 1992). The *in-situ* stress field of the crust is very complex and inhomogeneous, especially in areas adjacent to faults, which causes surrounding stresses to concentrate, attenuate, and even reverse (Zoback et al., 2002; Cornet and Röckel, 2012; Lin et al., 2013). Research on this topic began in the late 1970s; *in-situ* stress measurements were conducted around the sinistral strike-slip San Andreas fault zone located along the North American plate boundary with a total length of approximately 1287 km (Sbar et al., 1979; Zoback, 1980; Shamir and Zoback, 1992; Hickman and Zoback, 2004). The measurement results show that the orientation of the maximum horizontal principal stress is approximately perpendicular to the fault strike at distances of approximately 20 km away from the fault, which is consistent with the far-field stress. In contrast, it is nearly parallel to the fault strike within a distance of approximately 3 km from the fault. Additionally, the stress magnitude decreases as the distance from the fault decreases. The *in-situ* stress field of the approximately 2400-km long Tanlu fault zone, which passes through the eastern China plate, exhibits similar characteristics (Li et al., 1982; Feng et al., 2017). Some scholars have evaluated fault stability based on the *in-situ* stress measured around the fault zone. For example, in the southern section of the Tanlu fault zone, the stress accumulation is relatively high, indicating that this section is in a critically stable state, whereas the degree of stress accumulation around the Bohai, Liaoning, and Hebei sections are relatively low, indicating a relatively stable state (Liu et al., 2017; Feng et al., 2017; Qiu et al., 2019; Zhang et al., 2020).

Several *in-situ* stress measurements have been conducted along with intensive engineering construction in the eastern QTP since the 1980s, which provide an understanding of the stress state around the Xianshuihe fault. However, existing studies have mostly focused on the stress field near engineering construction sites (Wang et al., 2015; Ren et al., 2021; Xu et al., 2021; Suo et al., 2022), and there remains a lack of overall scientific analysis of the stress field and fault stability status of the XSHF. In this study, we first briefly describe the spatial distribution characteristics of the *in-situ* stress data and the Holocene activity of the XSHF and then analyze the stress field around the XSHF in detail based on *in-situ* stress data. Next, we discuss fault stability, seismic hazards along the XSHF, and the impact of XSHF activities on the uplift mechanism of the eastern QTP. The results will provide a better understanding of the relation between the stress field, the seismic activities of the strike-slip XSHF, and the mechanism of tectonic movement.

2 Geological background

2.1 Regional tectonic background and spatial distribution of Xianshuihe fault

The XSHF is an active block boundary fault developed on the southeastern margin of the QTP. It is a part of the Xianshuihe-Xiaojiang fault system, which consists of several other great faults, such as the Ganzi Yushu, Anninghe, Daliangshan, and Xiaojiang fault zones (Figure 1A) (King et al., 1997; Zhang, 2013). It acts as the southern boundary of the Bayan Har Block and the eastern boundary of the Sichuan-Yunnan Block (Allen et al., 1991; Chevalier et al., 2018). The tectonic stress field of this region is highly influenced by the northeastward intracontinental subduction of the Indian Plate and the clockwise rotation of the Sichuan-Yunnan Block, which resulted in the left-lateral strike-slip movement of the XSHF (Xie et al., 1995; Sheng et al., 2022).

The XSHF is slightly arc-shaped towards the northeast, with a total length of approximately 400 km, a strike of 40°–50° NW, and a dip of 55°–80° (Figure 1B) (Zhang G. et al., 2004; Bai et al., 2018). The fault zone is not continuous but incorporates several segments and can generally be divided into northwest and southeast sections by the Huiyuan Temple Basin. The northwestern section of the fault is developed in a slightly overlapping left-stepped echelon, and it can be divided into three segments from northwest to southeast: Luhuo segment (LHS), Daofu segment (DFS), Qianning segment (QNS). The southeastern section diverges through the Huiyuan Temple Basin to form multiple secondary faults, i.e., Zheduotang segment (ZDS)/Kanding segment (KDS)/Yalahe segment (YLS), the fault trace overlaps with Moxi segment (MXS) in Kangding area, and connects with the Anninghehe and Daliangshan fault zones near Shimian County (Figure 1B).

2.2 Slip rate and seismic activity along the fault since Holocene

The slip rate is one of the most significant indicators for evaluating the activity, accumulated strain energy, and seismic

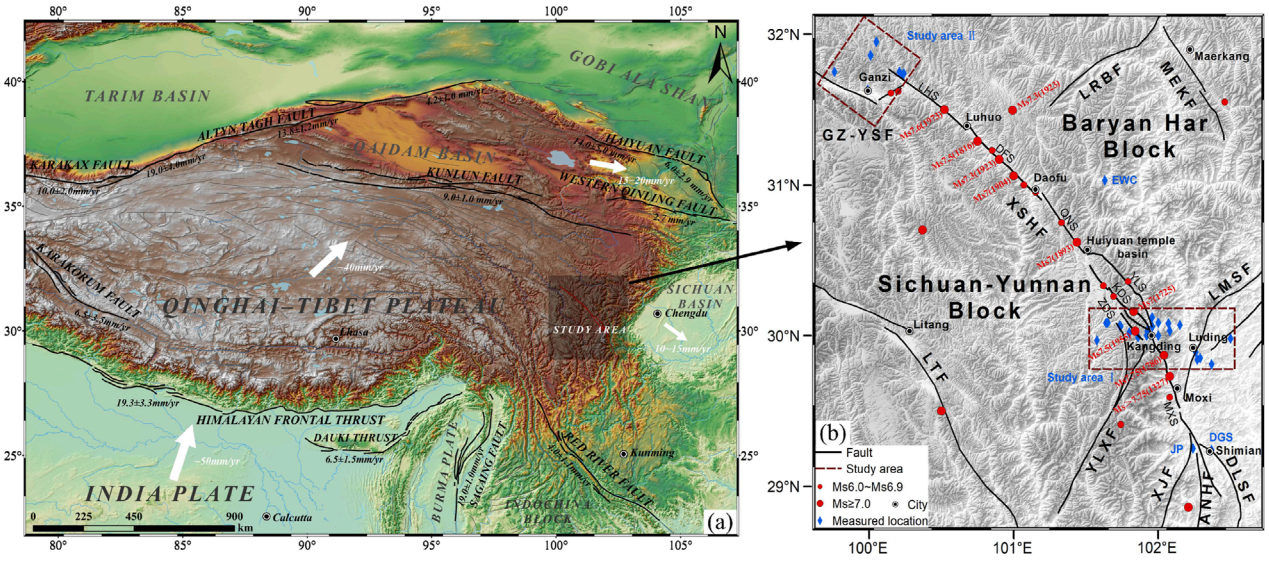

FIGURE 1
The geological background of XSHF. **(A)**The location of study area modified from (Tapponnier et al., 2001); **(B)** Spatial distribution and seismic development of XSHF(Stress measurements are from https://doi.org/10.12197/2023GA019); Historical earthquake data are from Wen et al. (2008) and the National Earthquake Data Center (https://data.arthquake.cn/). GZ-YSF-Ganzi-Yushu Fault; LMSF-Longmenshan Fault; XSHF-Xianshuihe Fault; DLSF-Daliangshan Fault; ANHF-Anninghe Fault; XJF-Xiaojiang Fault; LTF-Litang Fault; MEKF-Maerkang Fault; LRBF-Longriba Fault; YLXF-Yulongxi fault; LHS-Luhuo Segment; DFS-Daofu Segment; QNS-Qianning Segment; YLS-Yalahe segment; KDS-Salaha-Kangding segment; ZDS-Zhedotang segment; MGS-Mugecuo segment; MXS-MXS.

potential of a fault (Molnar and Tapponnier, 1978; Zhang et al., 2008; Liu et al., 2021). High slip rate indicates that the fault has strong activity and high accumulated strain energy (Li et al., 2018; Li et al., 2019), which can be used to determine fault stability and seismic hazard (Li et al., 2020). Several researchers have studied the Holocene slip rate of the XSHF (Table 1). The results show that the fault exhibits a shallow creep slip behavior, and the slip rate gradually increases from northwest to southeast along the fault (Zhang et al., 2018; Li et al., 2020; Qiao and Zhou, 2021; Li et al., 2022a; Zhang et al., 2022). Qiao and Zhou (2021) found a decrease in the strike-slip rate for the northwest segment. They inferred that the branch faults may have been locked, with a locking depth of approximately 7.6–18.5 km. The high creep-slip rate of the southeastern segment of the XSHF suggests high seismic hazard (Li et al., 2020), while the yearly decrease in slip rate and deeper locking in the northwestern segment of the XSHF also suggests possible seismic hazard (Qiao and Zhou, 2021).

As a boundary fault in the eastern QTP, the XSHF has observed strong seismic activities in the past centuries (Zhang et al., 2003). Since 1700, a total of nine earthquakes with Ms ≥ 7.0 and more than twenty earthquakes with Ms ≥ 6.0 have occurred along the fault (Wen et al., 2008; Bai et al., 2018). The seismic activity of the XSHF has been characterized by obvious periodic occurrences, that is, two active periods and one quiet period since 1700 (Papadimitriou et al., 2004; Wen et al., 2008; Zhang et al., 2016). The first active period lasted 116 years, from the Kangding Ms>6.5 earthquake in 1700 to the Luhuo Ms7.5 earthquake in 1816. The second active period lasted 129 years since the Huiyuan Temple Basin Ms7.0earthquake in 1893 (Wen et al., 2008). During these periods, several characteristic earthquakes occurred in the region, such as the 1816 (Ms7.5), 1923 (Ms7.3), and 1973 (Ms7.6) earthquakes in Luhuo and the 1725 (Ms7.0), 1786 (Ms7.75), and 1955 (Ms7.5) earthquakes in Kangding (Figure 2).

3 In-situ stress data

Several *in-situ* stress measurements have been conducted during engineering constructions or scientific investigations in the past decades, which facilitate the analysis of stress distribution characteristics around the XSHF. We collected 306 *in-situ* stress measurements from published literature and engineering reports since 1987. The *in-situ* stress data were measured using hydraulic fracturing (289), stress relief (9), and acoustic emission methods (8) at 46 sites near the fault, with the buried depth ranging from 5 m to 1305 m (Table 2, specific data sources can be accessed in Guo et al., 2023a). These *in-situ* stress data points were uniformly located, and mainly concentrated in two areas: 236 data points in study area I and 47 data points in study area II (Figure 1B). Study area I is located in the southeast section of the XSHF, near the intersection of the ZDS, KDS, YLS, and MXS, while study area II is located in the northwest section near the LHS. In addition, there are three other areas with relatively small numbers of stress data: the Jinping Village (JP) and Dagangshan hydropower station (DGS) areas with 18 data points in the southeast section of the MXS and the Erwacao hydropower station (EWC) area with five data points near the DFS (Figure 1).

TABLE 1 Strike-slip rate of different segments along XSHF (mm/yr).

Xianshuihe fault zone							References
Northwest section			Southeast section				
LHS	DFS	QNS	YLS	KDS	ZDS	MXS	
10–20				5			Qian (1988)
				5.5			Allen et al. (1991)
			1.8–2.2	4.9–6.1	3.3–3.9	9.3–10.5	Zhou et al. (2001)
10–11							Shen et al. (2005)
15.1			4–6				Wang et al. (2008)
9–12							Wang et al. (2009)
8.7–10.3	7.7–8.8	7.3–8.3	7.1–7.6	7.0–7.4		7.2–14.7	Jiang et al. (2015)
4.6–12							Yan and Lin, (2015), Yan and Lin, (2017)
7.67–9.13			4.41–6.14				Li et al. (2019)
8.12–9.3							Sun et al. (2021)
9.4	8.8–9.4	9.9–14.3				17.9	Qiao and Zhou (2021)

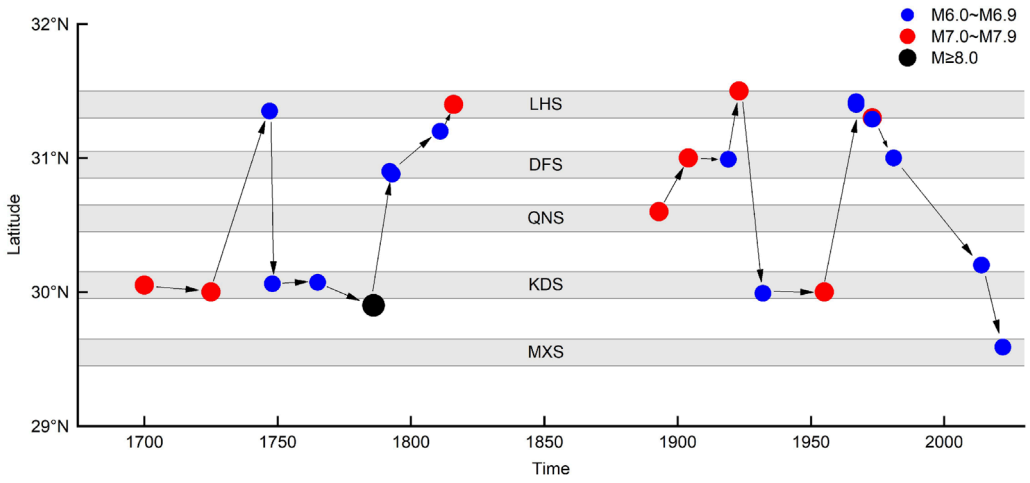

FIGURE 2
Spatial-temporal distribution of M ≥ 6.0 earthquakes in XSHF.

4 Results

4.1 The stress magnitude with depth

We analyzed the distribution characteristics of *in-situ* stress surrounding the fault zone. The horizontal and vertical principal stress components with respect to the buried depth are shown in Figure 3. The results indicate that, in general, the maximum horizontal principal stress σ_H dominates the stress field close to the XSHF at depths shallower than 1400 m, having a stress magnitude of 1.7–53.5 MPa. We further investigated the stress fields of study areas I and II to understand the effects of different locations around the fault. In study area I, the *in-situ* stress magnitudes are very discrete at shallow depths, especially at depths shallower than 400 m (Figure 3B). According to the Andersons' fault stress model (Anderson, 1951), the stress state in each area

TABLE 2 The collected *in-situ* stress data around XSHF (detailed data can be accessed in Guo et al., 2023a).

Location	Measurement approaches	Number of sites	Number of tests	Depth (m)	σ_H	
					Magnitude (MPa)	Direction (°)
Study area I	Hydraulic fracturing, stress relief, acoustic emission method	35	236	5–1305	1.7–53.5	1–171
Study area II	Hydraulic fracturing	7	47	15–236	3.7–19.8	20–80
EWC	Hydraulic fracturing	1	5	408–424	8.4–13.1	155–160
JP-DGS	Hydraulic fracturing, stress relief	3	18	97–400	7.6–22.04	15–176

determines the fault types, namely, strike-slip, reverse, and normal types. At depths greater than 400 m, the vertical stress component gradually becomes the intermediate principal stress, indicating that the fault type at greater depths is mainly strike-slip. The southeastern segment of the XSHF in study area I is located at the intersection of the Y-shaped tectonic zone, which is one of the most active areas in the world, resulting in an extremely complex shallow crustal stress state. In study area II, the *in-situ* data were obtained mainly within a depth of 250 m (Figure 3C). The stress field characterized ($\sigma_H > \sigma_h > \sigma_V$) by the *in-situ* stress data indicates an inverse faulting stress regime. However, the seismic source mechanism solution reflects a normal fault stress state around the step over between the Yushu fault and XSHF with left-lateral strike-slip motion (Zhou et al., 1983; Wen et al., 2008). This indicates a complex stress state near the fault tip, coupled with topography and geomorphology at shallow depths (e.g., Liu et al., 2005; 2011). Previous studies have reported a similar phenomenon in other pull-apart basins, for example, a reverse fault stress state exists in the basin formed by step over Haiyuan strike-slip fault (Lin et al., 2017; Lei et al., 2021).

The slope of the regression line shows that the change gradients of σ_H, σ_h, and σ_V in study areas I and II are 3.23 MPa, 2.57 MPa, and 2.68 MPa and 6.47 MPa, 4.68 MPa, and 2.61 MPa per 100 m, respectively. The magnitude of the maximum horizontal principal stress component in study area I is 3.3564 MPa, which is greater than that in study area II (2.8931 MPa), indicating that the horizontal tectonic stress near the Earth's surface is stronger in the southeastern section.

To further analyze the relationship between the horizontal and vertical stresses at different depths around the fault zone, the lateral pressure coefficient K_{av} proposed by Brown and Hoek (1978) was adopted (Eq. 1), as shown in Figure 4. The results indicate that the lateral pressure coefficient is relatively discrete at shallow depths. As the buried depth gradually increases, K_{av} gradually converges to approximately 1.03, which is slightly greater than 1.0, indicating that the horizontal stress dominates the stress field within the depth considered in this study. Previous studies have shown that the lateral pressure coefficient K_{av} of the Sichuan-Yunnan block tends to be 0.95 within a buried depth of 1200 m (Zhang et al., 2022) and that of the middle China North-South Seismic Belt tends to be 0.628 within a buried depth of 749 m (Yang et al., 2012). A comparison of K_{av} between the XSHF and the other two zones indicates that the XSHF and the adjacent areas withstand stronger horizontal compression. The stress state of the southeastern segment of the fault zone (Study area I, Figure 4B) is more complex than that of the northwestern segment (study area II, Figure 4C), which may be mainly due to the intense tectonic activities and the steeper and higher terrain in study area I. The Earth's surface processes have substantial effects on the stress field within a certain buried depth close to the Earth's surface.

$$K_{av} = \frac{(\sigma_H + \sigma_h)}{2\sigma_V} \tag{1}$$

where K_{av} is the lateral pressure coefficient; σ_H is the maximum horizontal principal stress (MPa); σ_V is the vertical stress (MPa); σ_h is the minimum horizontal principal stress (MPa).

4.2 Stress magnitude with fault distance

To analyze the change characteristics of the *in-situ* stress at different locations around the fault zone, it is necessary to ensure that the buried depths of the *in-situ* stress measurement points are at the same level. Therefore, we converted the *in-situ* stresses at different depths to those at the Earth's surface using Eq. 2 (Brady and Brown, 2006). We obtained the values of maximum shear stress τ_m at each measuring position using Eq. 3, which are equal at either buried depth according to Eq. 2 (Jaeger et al., 2009).

$$\sigma_{Ho} = \sigma_H - k\gamma h \tag{2}$$

$$\tau_m = \frac{\sigma_1 - \sigma_3}{2} \tag{3}$$

where k and γ denote the coefficient of lateral pressure and gravity (kN/m^3) respectively; h is depth (m); σ_H, τ_m, σ_1, and σ_3 are the maximum horizontal principal stress, maximum shear stress, and maximum and minimum principal stress (MPa), respectively; σ_{Ho} is the maximum horizontal principal stress (MPa) at the Earth's surface.

In study area I, the fault segment is composed of four branched faults, the ZDS, KDS, YLS, and MXS, from southwest to northeast (Figure 1). We found that the maximum horizontal principal stress presents a hump shape on both sides of the

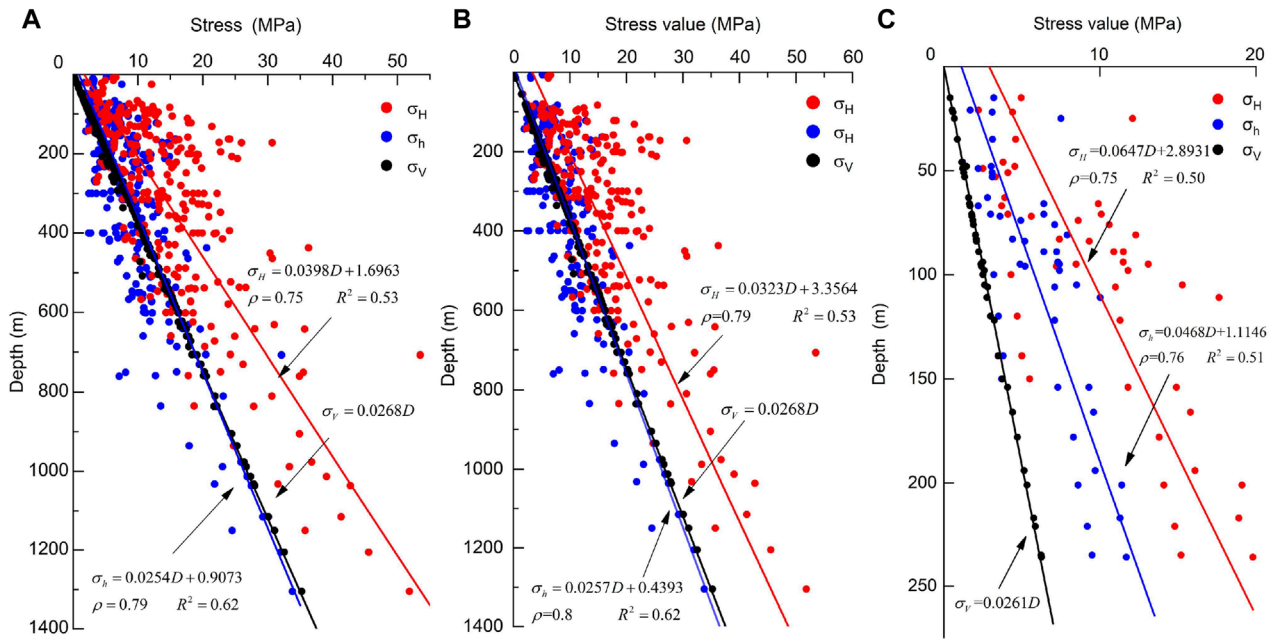

FIGURE 3
The *in-situ* stress magnitude with depth: **(A)** total; **(B)** study area I; **(C)** study area II.

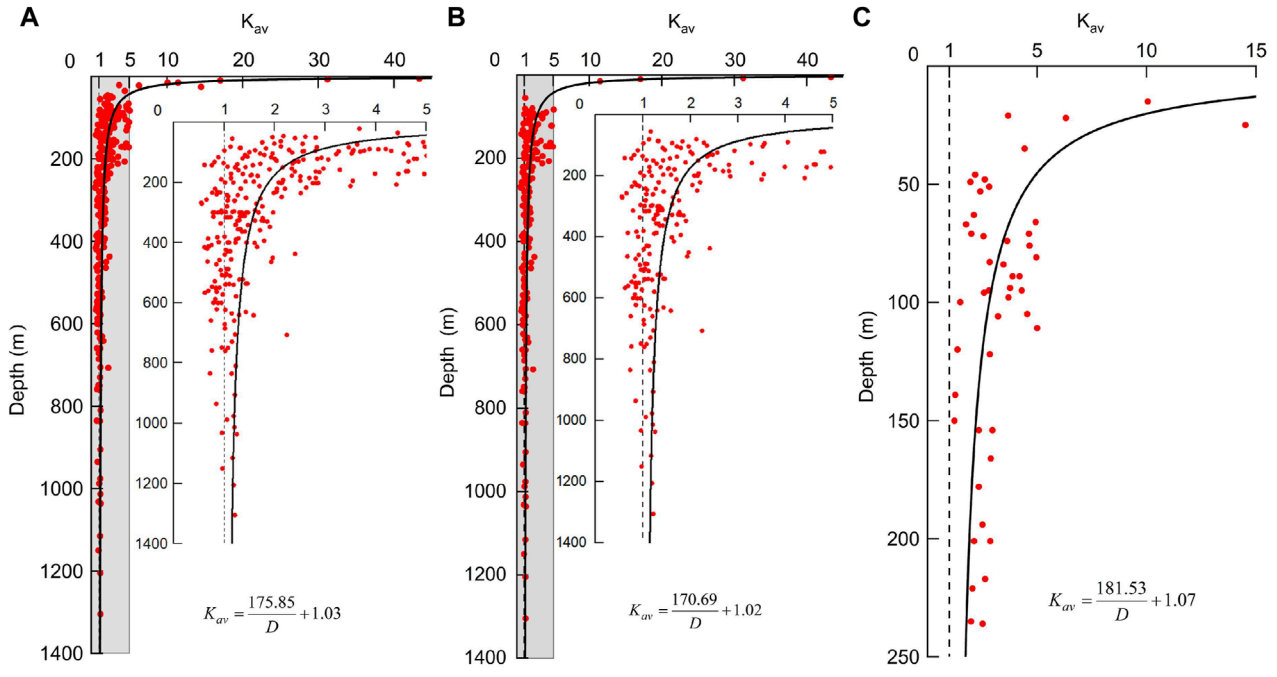

FIGURE 4
Distribution of lateral pressure coefficient with depth: **(A)** total; **(B)** study area I; **(C)** study area II.

fault zone, which can be depicted as a double-hump-type stress field (Figure 5A). There is a low stress zone (hump valley) between YLS and ZDS; as the distance increases from the YLS and ZDS, the stress magnitude gradually increases on both sides and reaches a peak (hump), then decreases and eventually stabilizes. We calculated the maximum shear stress and obtained its average magnitude at different buried depths for each site. As the fault distance increases, the magnitude of

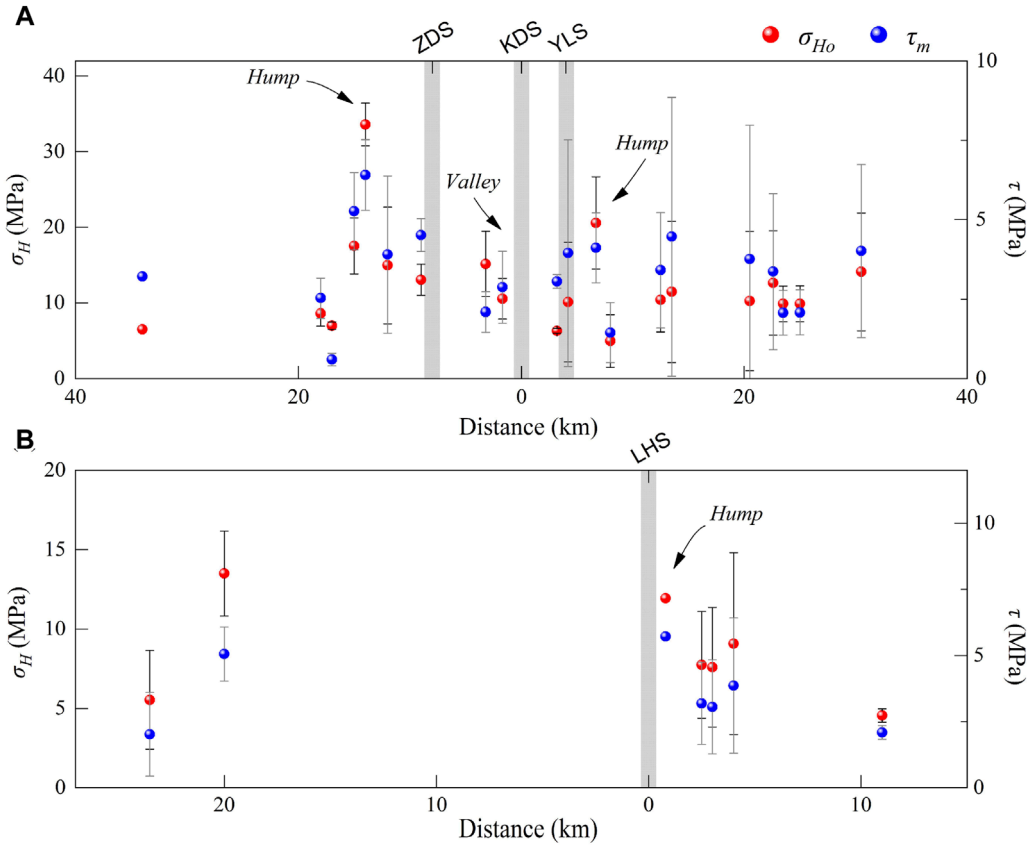

FIGURE 5
Distribution of maximum horizontal stress (σ_{Ho}) and shear stress (τ_m) with fault distance: **(A)** σ_{Ho} and τ_m in study area I; **(B)** σ_{Ho} and τ_m in study area II.

the maximum shear stress also shows a similar "double hump" trend (Figure 5B). However, the stress field around the LHS in study area II is not as complex as that in study area I. This indicates that the maximum horizontal principal stress exhibits a "single hump" distribution feature. The stress magnitude reaches a hump near the fault zone, decreases gradually, and then tends to be consistent with the far-field stress field with an increase in the fault distance (Figures 5A, B). The results indicate that the stress always increases near the fault zone, generally within the relatively intact host rocks neighboring the fracturing rocks. The double and single humps near the fault zone primarily stem from the width of the fault zone. A wider fault zone leads to a reduction in stress in the fractured rock mass (Sibson, 1980; Weng et al., 2020).

We interpolated the *in-situ* stress using the inverse distance weighting method of ArcGIS and obtained the stress contours for study areas I and II (Figures 6A, B). In study area I, a stress concentration (14.3–33.6 MPa) occurs at the southwestern side of the fault tip (the red area of the ZDS in Figure 6A), while a stress relaxation (4.5–9.1 MPa) occurs at the northeastern side of the fault tip (the green area of the YLS in Figure 6A). Such stress distributions mainly result from the movement of the left lateral strike-slip fault zone. The stress concentration and relaxation areas around the southeastern fault zone correspond to the Minya Konka and Yalahe valleys, respectively (Wen and Bai, 1985), which may indicate the possible effect of the sinistral strike-slip on the formation of the geomorphology around the fault tip (Figure 6C) (Guo et al., 2016). In study area II, a significant stress variation is observed around the fault tips, reflecting the influence of the fault zone on the surrounding stress field.

4.3 Stress orientation surrounding the fault zone

At locations near active faults, the stress orientation is often deflected and inconsistent with the regional stress field, and it is important to understand the stress disturbance around faults, which is still less understood (Zoback, 1992; Chang et al., 2010). We plotted the *in-situ* maximum horizontal principal stress orientations around the fault zone and the three stress zones using a rose diagram (Figure 7). The results showed that the dominant stress orientation in Baryan Har stress zone (B217)、Longmengshan-Songpan stress zone (B218) and Sichuan-Yunnan stress zone (B219) are 20–40°NE, 280–320°NWW and 290–310°NWW, respectively (Figure 7A). The dominant stress orientation near the northwest tip of the fault is approximately 50°–70° NEE, holding a large intersection angle with the fault. The stress orientation on the

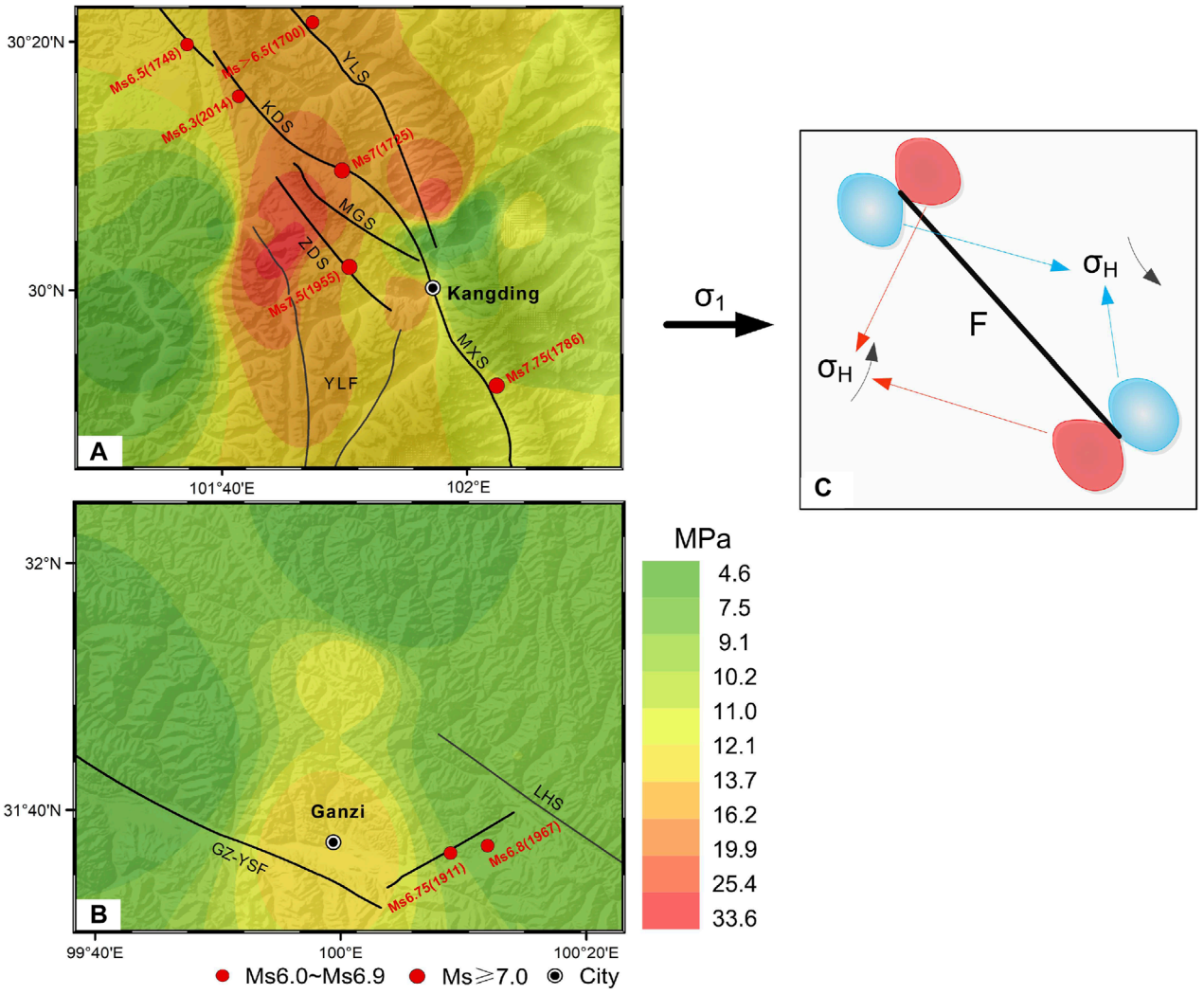

FIGURE 6
Maximum horizontal stress contours around fault segments: **(A)** study area I; **(B)** study area II; **(C)** stress disturbance around the sample with cracks. F denotes preexisting fault, and σ_1 denotes far-field principal compressive stress (Modified from Guo et al. (2016)).

two sides of the fault zone is generally in the NW direction, which is in accordance with the fault strike. The dominant stress orientation near the southeastern tip of the fault is NE, which is nearly perpendicular to the fault. Overall, the orientation of the maximum horizontal principal stress exhibits an elliptical shape around the XSHF, which is significantly different from the dominant stress orientation of the three neighboring stress zones. (Figure 7). This type of stress distribution has been reported in several studies (Yale et al., 1994; Scholz, 2000; Su, 2002; Yale, 2003; Zhao et al., 2013). In the elliptical-shaped stress field, the stress orientations exhibit a deflection of approximately 30° between the two sides of the fault in study area I, and the largest deflection occurs around the southeastern tip, reaching nearly 90°. Such a deflection of the nearby stress orientation may result from the extreme heterogeneity in the mechanical properties of the fault zone, fractured rocks, and nearby undisturbed host rock mass (Hudson and Cooling, 1988; Hardebeck and Hauksson, 1999; Provost and Houston, 2001; Su et al., 2003).

The *in-situ* stress analysis indicates that the local stress field around the XSHF is highly disturbed, which may be influenced by a series of factors, such as fault properties, fault spatial distribution, and tectonic activity intensity.

5 Discussion

5.1 Seismogenic potential assessment based on the stress state

High ground stress tends to drive fault slip and trigger earthquakes (Elsworth et al., 2016). Near the LHS, ZDS, YLS, and MXS, the σ_H and τ_m are relatively high compared with the far-field stress. The stress concentration around the tips or intersections of fault segments provides the requisite conditions for earthquakes, i.e.,

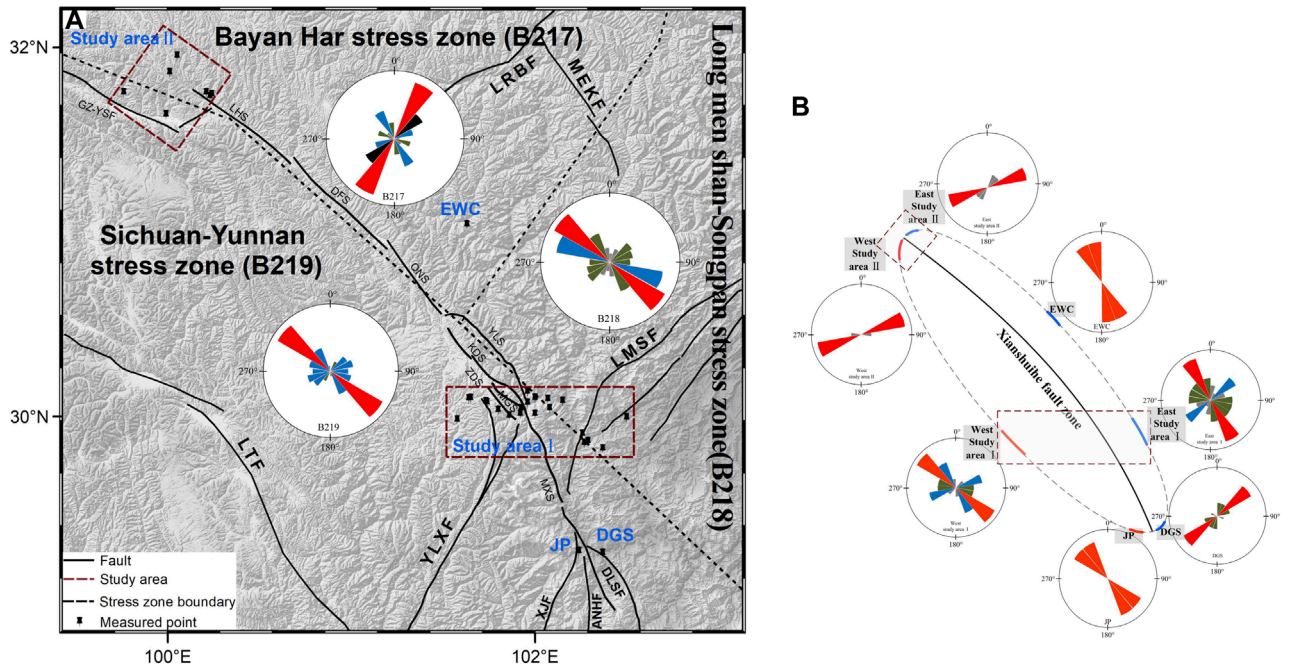

FIGURE 7
Rose diagram of the maximum horizontal principal stress orientation around the XSHF **(A)** Three stress zones (detailed data can be accessed in Guo et al., 2023b); **(B)**. Schematic diagram of the elliptical-shaped stress field. (The red fan-shaped in the rose diagram indicates the regional dominant orientation; the red and blue solid lines indicate the stress orientation at the measured points on the west and east sides of the XSHF, respectively, the gray dashed line indicates elliptical-shaped stress orientation around the XSHF).

study areas I and II. In fact, over half of the historical earthquakes in the XSHF with Ms ≥ 6.0 occurred in these areas (Figures 6A, B).

The sliding potential of a fault is defined by the ratio of the shear stress τ to the normal stress σ acting on the fault (Eq. 4; Morris et al., 1996). When the shear stress τ reaches its sliding resistance, the fault slips, converting the accumulated strain energy into kinetic energy and thereby causing crustal deformation and even earthquakes (Tanaka et al., 1981; Wang et al., 2012). According to Jaeger et al. (2009), the ratio μ_m of the maximum shear stress τ_m to the maximum normal stress σ_m can be expressed as a function of the friction coefficient μ (Eq. 5). The pore water pressure P_0 is also considered because it can weaken the effective normal stress (Chang et al., 2010).

$$\tau = \mu\sigma = \tan\varphi\sigma \tag{4}$$

$$\mu_m = \tau_m/(\sigma_m - P_0) = (\sigma_1 - \sigma_3)/(\sigma_1 + \sigma_3 - 2P_0) = \mu/\left[(1+\mu^2)^{1/2}\right] \tag{5}$$

where σ_1 and σ_3 are the maximum and minimum principal stresses acting on the fault plane, respectively; P_0 denotes the pore pressure, which can be approximately represented by water column static pressure, i.e., $P_0 = \rho h$ in this study, where ρ and h denote the density of water and buried depth, respectively.

The larger μ_m signifies a higher degree of stress accumulation, and when the stress level along a fault reaches a threshold value, the stress is released through fault activity, and then μ_m decreases to maintain the stability of the crust (Zhang et al., 2022). Townened (2000) analyzed boreholes drilled data and found that the stress magnitudes are consistent with Coulomb frictional-failure theory for coefficients of friction of 0.6–1.0 such as are measured experimentally in laboratory settings (Byerlee, 1978), and noted that the stress accumulation degree is high when μ_m between 0.5 and 0.7, and that faults are susceptible to sliding instability when μ_m exceeds 0.7 (Townened and Zoback, 2000). However, some studies have indicated that the friction coefficient of fault rocks can weaken to approximately 0.2 due to special composition of the fault gauge (Qin et al., 2014). and Li et al. (2018) showed that when μ_m is between 0.2 and 0.5, the stress intensity is low and the chance of fault reactivation is small, and when μ_m is less than 0.2, the fault is in a stable state. Accordingly, we calculated using Equation 5 that the range of μ_m to cause fault activity and evaluate the degree of stress accumulation and stability of the fault zone (Table 3).

It is important to note that the present evaluation approach does not consider the spatial relationship between the fault strike and the axis of the maximum principal stress; therefore, the slip trend obtained represents the maximum magnitude, which may lead to an overestimation of the seismic hazard. In addition, the depths of *in-situ* stress measurements are limited to 2000 m, whereas earthquakes mostly occur at depths of approximately 10 km. The high stress at shallow depths always reflects the high stress at greater depths. Thus, we hypothesize that the stresses at shallow depths (<2000 m) and great depths (~10 km) are coupled with each other (Li et al., 2023).

We calculated the effective normal stress and shear stress based on the measured stress data and then evaluated the degree of stress accumulation at each measuring position (Figure 8). On this basis, we discuss the degree of stress accumulation at

TABLE 3 Classification for stress accumulation degree and fault stability (Townened and Zoback, 2000; Li et al., 2018).

μ_m	Stress accumulation classification	Fault stability depiction
>0.7	Very high	Unstable, prone to sliding
0.5–0.7	High	In critical state
0.2–0.5	Moderate	Relatively stable
<0.2	Low	stable

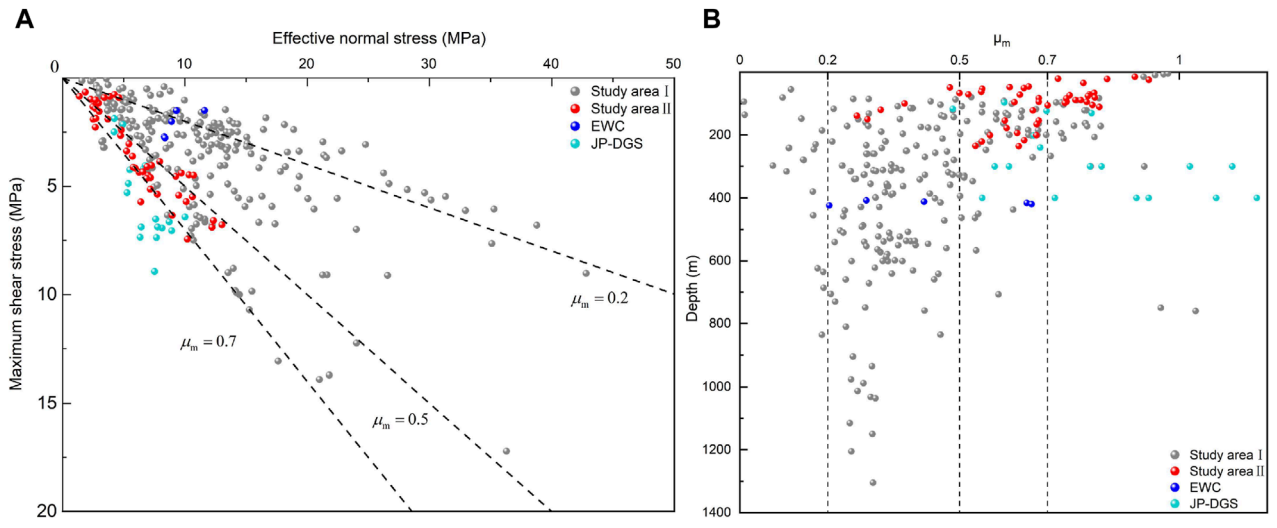

FIGURE 8
Stress accumulation characteristics of different locations around the fault. **(A)** Ratios of effective normal stress with shear stress; **(B)** the degree of stress accumulation with buried depth.

different fault segments of the XSHF, i.e., Luhuo segment, Daofu-Qianning segment, Zheduotang- Kangding- Yalahe segment, and Moxi segment from northwest to southeast.

5.1.1 Luhuo segment

The stress accumulation at most of the measuring points in study area II, near the northwestern tip of the fault zone, was classified as high or very high (μ_m>0.5). Although the buried depths of the measuring points are generally shallow (mostly <300 m) (Figure 8, Figure 9B), the high degree of stress accumulation indicates that the LHS possesses a high sliding potential. In addition, it has been 50 years since the 1973 M7.6 earthquake, which is close to the 50-year elapsed time of the last two characteristic earthquakes that occurred in 1923 and 1973. This indicates the possibility for a characteristic earthquake to occur in the near future.

5.1.2 Daofu-Qianning segment

The Daofu-Qianning Segment is located in the middle of the fault zone. The limited stress data in the EWC measuring point shows that the degree of stress accumulation around this segment is mostly classified as medium or low (μ_m < 0.5), not as high as that of LHS. However, based on the analysis of the elapsed time and the amount of dislocation loss, Bai et al. (2022) observed the earthquake potential of this segment for strong earthquakes above Ms6.8, which can be used for reference.

5.1.3 Zheduotang-Kangding-Yalahe segment

The Zheduotang-Kangding-Yalahe segment is located in the southeastern fault zone and consists of three sub-parallel branch faults, as shown in study area I. The degree of stress accumulation in this area tends to decrease with an increase in buried depth. The measuring points with very high- and high-stress accumulation (μ_m>0.5) extend from the surface to a depth of approximately 800 m, indicating that this segment has accumulated a high amount of energy. Furthermore, the stress accumulation presents a double-hump feature in the section perpendicular to the fault (Figure 9A). The degree of stress accumulation is moderate or low (μ_m < 0.5, valley) near the KDS and MXS which are located in the middle of the three branch faults. However, the degree of stress accumulation is very high (μ_m > 0.7, camel hump) near the northeast YLS, high (0.5<μ_m<0.7, camel hump) near the southwest ZDS, and decreases to a moderate degree when far away from the fault zone (0.2<μ_m<0.5).

The Zheduotang-Kangding-Yalahe segment has witnessed several large historical earthquakes. There were five earthquakes greater than Ms6.0 during the 116-year period from 1700 to 1816

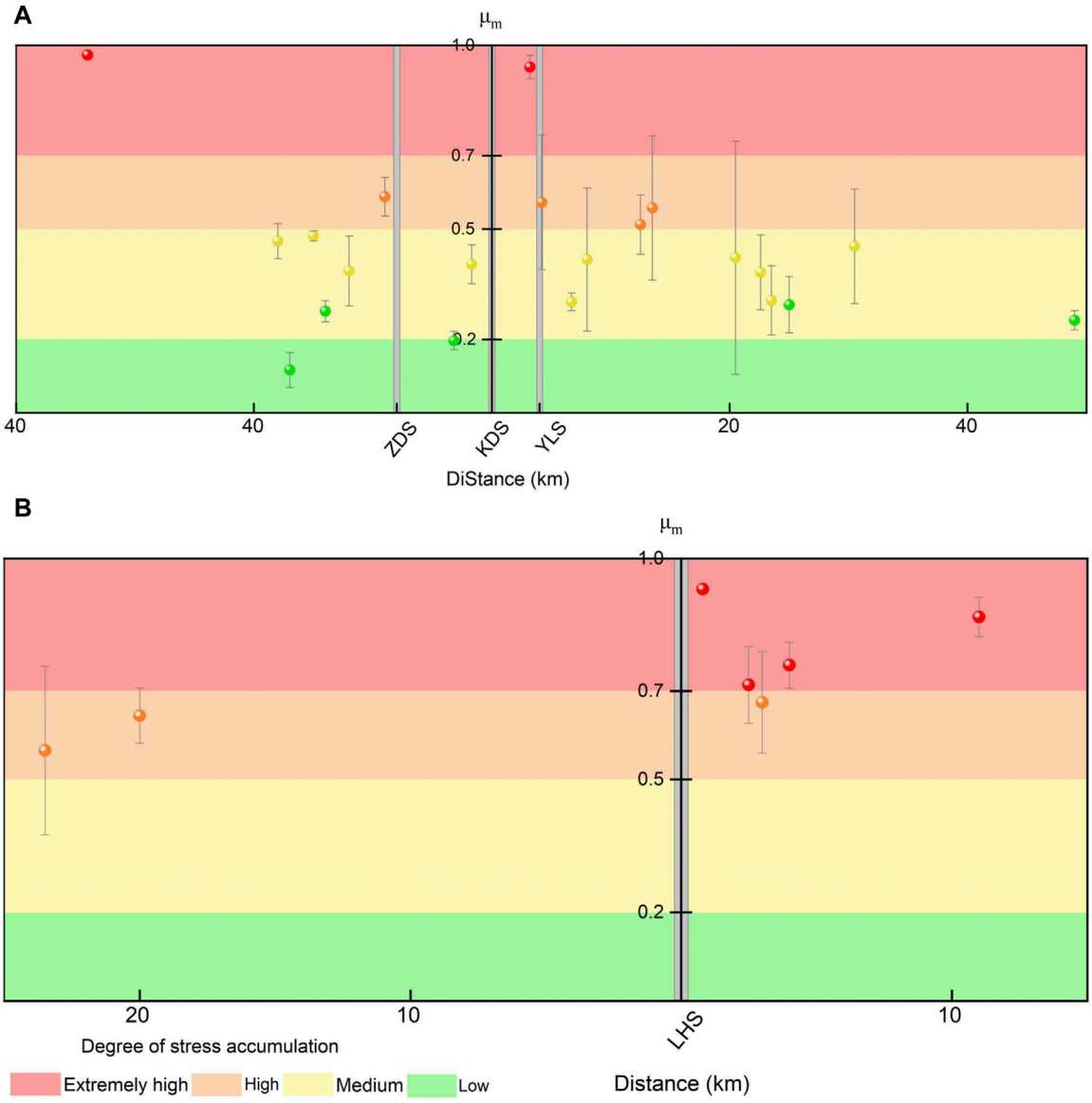

FIGURE 9
Distribution of stress accumulation degrees with fault distance: **(A)** study area I; **(B)** study area II (Red, orange, yellow and green dots indicate extremely high, high, medium and low stress accumulation, respectively, which is calculated according to Eq. 5).

and two earthquakes since 1950, i.e., Ms7.5 and Ms6.3 in 1955 and 2014, respectively. Considering the recurrence period of 260 years in the Kangding area and the last earthquake of Ms 7.75 in 1786, the ZDS has a high potential for strong earthquakes of M6.9 ± 0.3 (Wen et al., 1989; Ma et al., 2022). All these indicate that this segment has a high potential for strong earthquakes.

5.1.4 Moxi segment

The MXS is the southeastern segment of the XSHF. Based on the *in-situ* stress measured from the JP-DGS area, all the measuring points are characterized by a high or very high degree of stress accumulation (μ_m > 0.5), indicating that the MXS is in a critical or unstable state. Currently, earthquakes are frequently occurring in this area, e.g., 2022 M6.8 and 2023 M5.6, confirming the high seismic potential of the area.

Our analysis shows that the LHS, YLS, ZDS, and MXS have high degree of stress accumulation. The local stress around the fault is always higher than the far-field stress, which is in accordance with the stress distribution characteristics noticed around many other faults before earthquakes, such as the 1995 Hyogo Ms7.2 earthquake and the 2008 Wenchuan Ms8.0 earthquake (Tanaka et al., 1998; Guo et al., 2009). The "Static Stress-Tiggering Hypothesis" states that the interaction between faults will cause a change in seismic potential (King et al., 1994; Hodgkinson et al., 1996; Hardebeck et al., 1998; Zhang et al., 2003; Wen et al., 2008). Therefore, the occurrence of the Luding earthquake in 2022 in the

MXS is likely to cause an increase in coseismic Coulomb stress of nearby branch faults in the XSHF. Therefore, full attention should be paid to the potential seismic hazards in high-stress areas, including the ZDS, YLS, MXS, and LHS.

5.2 Implications for the regional tectonic movement

Dynamic models depicting the uplift of the southeastern QTP mainly include the lateral extrusion of rigid blocks (Tapponnier et al., 2001), lower crustal flows (Royden et al., 1997), and continuous deformation of the entire lithosphere (Molnar and Tapponnier, 1975; Houseman and England, 1993). The lateral extrusion of rigid blocks refers to the boundary force driven by the uplift deformation of the QTP resulting from the India–Eurasia collision. The rigid block is compressed and uplifted due to the movement of the strike-slip boundary faults in the southeastern QTP (Tapponnier et al., 1982; Peltzer and Saucier, 1996; Peltzer and Tapponnier, 1998; Calais et al., 2006). The lower crust flow model is driven by gravity generated by the crustal thickening of the central QTP. The weak viscous layer moves outward from the central plateau through the lower crust as a channel with uniform thickness and causes crustal uplift around the strong Sichuan and Tarim Basins (Block and Royden, 1990; Clark and Royden, 2000). Because different dynamic models correspond to stresses caused by different sources, the stress distributions can provide the information for clarifying the dynamic models for the plateau crust.

The *in-situ* stress field shows that the horizontal stress is always the dominant stress around the XSHF (Figure 3). The stress state in the region is characterized by strike-slip with thrust, which is consistent with previous studies that the sinistral strike-slip and thrust movements are the main crustal deformation processes in the eastern margin of the QTP (Molnar and Tapponnier, 1975; Tapponnier et al., 2001; Li et al., 2022b). Further, when the rigid crust constrains the strike-slip fault movements, the adjacent crustal rock mass is laterally shortened by translational compression (Harland, 1971; Sanderson and Marchini, 1984), followed by compensatory tectonic uplift (Lowell, 1972; Wilcox et al., 1973; Bartlett et al., 1981). Meanwhile, the study indicated that strain rate field shows highly localized shear strain along the Xianshuihe fault zone (Li et al., 2019). The results of terminating crustal extrusion near the margin of southeastern Tibetan Plateau are consistent with the decreasing slip rates along the Xianshuihe fault zone (Zheng et al., 2017), where strain localization along the major strike-slip faults ends and transfers to crustal compression and thickening. The geomorphological characteristics of the rapidly uplifting Minya–Konka fault block in this area are consistent with this process (Wen and Bai, 1985). Similar conclusion has been reached by studies in northeastern Tibetan Plateau (Li et al., 2018). Moreover, the geometric spatial distribution of the XSHF is similar to the geometric shape of the slip line in the plane indentation plasticity problem (Figure 10), and the SE–NW oriented regional horizontal principal stress direction distribution may also be related to the indentation effect caused by the India–Eurasia collision (Tapponnier and Molnar, 1976; Sylvester, 1988). The above analysis shows that the study area is controlled by strong horizontal tectonic movement caused by the India–Eurasia collision. Based on the characteristics of the stress field, the tectonic uplift of the southeastern margin of the QTP appears to be more consistent with the rigid lateral compression dynamic model.

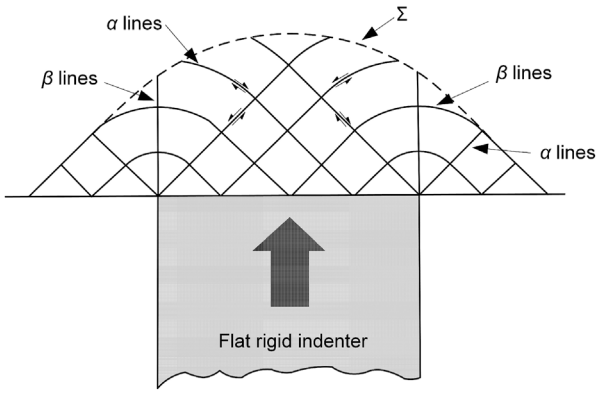

FIGURE 10
Slip line field and plastic zone of the indentation yield point of a plane rigid block in a semi-infinite medium. This figure is modified from Tapponnier and Molnar (1976); Σ denotes the possible plastic boundary at the yield point, and α and β slip lines denote the two orthogonal families of curves.

6 Conclusion

In this study, we analyzed the distribution characteristics of the stress magnitude, orientation, and accumulation degree based on a series of *in-situ* stress data collected for the XSHF. Based on the stress data, the fault stability and seismic hazards of each fault segment were evaluated. The main conclusions are summarized as follows:

1) The stress field around the XSHF is extremely complex, especially at shallow depths near the Earth's surface, caused by geomorphic stress and tectonic activities. The coexistence of the strike-slip, thrust, and normal stress states indicates multiple types of fault movements at different fault locations. Horizontal stress dominates the stress field, and in the southeastern parts of the fault zone, the fault movement becomes purely strike slip at great depths, i.e., at depths more than 400 m.
2) The stress field around the fault was significantly different from the regional stress field. "Elliptical" stress fields were formed on both sides of the fault zone, and the magnitude of the stress is characterized by single or double hump-like as distance increases from the fault. The material heterogeneity of the fault zone and its adjacent host rocks controls the local stress field, resulting in the decoupling or rotation of the local stress near the fault. This study shows that the stress measured within a specific range of the fault zone does not represent the regional stress; however, regional stress has some implications for *in-situ* stress measurements.
3) The degree of stress accumulation are classified as high or very high in some fault segments: LHS, ZDS, YLS, and MXS.

Such a high degree of stress accumulation indicates a critically unstable or prone to sliding state of fault segments. A comprehensive analysis indicates that ZDS, YLS, and LHS have a relatively high potential for strong earthquakes.

4) The stress-based analysis shows that the study area is dominated by the strong horizontal tectonic movement generated by the India–Eurasia collision and that the regional tectonic uplift is more in line with the rigid lateral compression dynamic model.

Data availability statement

The original contributions presented in the study are included in the article/Supplementary material, further inquiries can be directed to the corresponding author.

Author contributions

SG: Conceptualization, Formal Analysis, Funding acquisition, Investigation, Methodology, Project administration, Supervision, Writing–original draft, Writing–review and editing. JL: Data curation, Investigation, Methodology, Writing–original draft. SQ: Conceptualization, Methodology, Project administration, Writing–review and editing. BZ: Investigation, Writing–review and editing. YaZ: Supervision, Validation, Writing–review and editing. YuZ: Writing–review and editing. WZ: Validation, Writing–review and editing. FW: Data curation, Writing–original draft. KZ: Writing–review and editing.

Funding

The author(s) declare that financial support was received for the research, authorship, and/or publication of this article. The achievements described in this paper have been supported by the National Natural Science Foundation of China (41825018, 42077266, and 42207205), the Second Tibetan Plateau Scientific Expedition and Research Program (2019QZKK0904), the National Key Research and Development Program of China (2023YFC3012004-05), and the Youth Innovation Promotion Association of the Chinese Academy of Sciences (2022062).

Conflict of interest

The authors declare that the research was conducted in the absence of any commercial or financial relationships that could be construed as a potential conflict of interest.

Publisher's note

References

Alexander, L. G. (1997). *The near surface stress field near the site of the 1969 meckering earthquake*. Durham: IASPEL and IAVCEI, Joint general assemblies. Western Australia.

Allen, C. R., Luo, Z. L., Qian, H., Wen, X. Z., Zhou, H. W., and Huang, W. S. (1991). Field study of a highly active fault zone: the Xianshuihe fault of southwestern China. *Geol. Soc. Am. Bull.* 103 (9), 1178–1199. doi:10.1130/0016-7606(1991)103<1178:fsoaha>2.3.co;2

Anderson, E. M. (1951). The dynamics of faulting. *Trans. Edinb. Geol. Soc.* 8, 387–402. doi:10.1144/transed.8.3.387

Bai, M., Chevalier, M., Li, H., Pan, J., Wu, Q., Wang, S., et al. (2022). Study on late Quaternary strike-slip rate and regional strong earthquake risk of Qianning section of Xianshuihe fault zone. *J. Geol.* 96 (07), 2312–2332. doi:10.3969/j.issn.0001-5717.2022.07.005

Bai, M., Chevalier, M. L., Pan, J., Replumaz, A., Leloup, P. H., Métois, M., et al. (2018). Southeastward increase of the late Quaternary slip-rate of the Xianshuihe fault, eastern Tibet. Geodynamic and seismic hazard implications. *Earth Planet. Sci. Lett.* 485, 19–31. doi:10.1016/j.epsl.2017.12.045

Bartlett, W. L., Friedman, M., and Logan, J. M. (1981). Experimental folding and faulting of rocks under confining pressure Part IX. Wrench faults in limestone layers. *Tectonophysics* 79 (3-4), 255–277. doi:10.1016/0040-1951(81)90116-5

Block, L., and Royden, L. H. (1990). Core complex geometries and regional scale flow in the lower crust. *Tectonics* 9 (4), 557–567. doi:10.1029/tc009i004p00557

Brady, B. H. G., and Brown, E. T. (2006). *Rock mechanics: for underground mining*. Springer science and business media.

Brown, E. T., and Hoek, E. (1978). Trends in relationships between measured *in-situ* stresses and depth. *Int. J. Rock Mech. Min. Sci. Geomechanics Abstr. Pergamon* 15 (4), 211–215. doi:10.1016/0148-9062(78)91227-5

Byerlee, J. O. (1978). Friction of rocks. *Pageoph* 116 (4/5), 615–626. doi:10.1007/bf00876528

Calais, E., Dong, L., Wang, M., Shen, Z., and Vergnolle, M. (2006). Continental deformation in Asia from a combined GPS solution. *Geophys. Res. Lett.* 33 (24). doi:10.1029/2006gl028433

Chang, C., Lee, J. B., and Kang, T. S. (2010). Interaction between regional stress state and faults: complementary analysis of borehole *in situ* stress and earthquake focal mechanism in southeastern Korea. *Tectonophysics* 485 (1-4), 164–177. doi:10.1016/j.tecto.2009.12.012

Chevalier, M. L., Leloup, P. H., Replumaz, A., Pan, J., Métois, M., and Li, H. (2018). Temporally constant slip rate along the Ganzi fault, NW Xianshuihe fault system, eastern Tibet. *Bulletin* 130 (3-4), 396–410. doi:10.1130/b31691.1

Clark, M. K., and Royden, L. H. (2000). Topographic ooze: building the eastern margin of Tibet by lower crustal flow. *Geology* 28 (8), 703–706. doi:10.1130/0091-7613(2000)028<0703:tobtem>2.3.co;2

Cornet, F. H., and Röckel, T. (2012). Vertical stress profiles and the significance of "stress decoupling". *Tectonophysics* 581, 193–205. doi:10.1016/j.tecto.2012.01.020

Duan, B. (2010). Role of initial stress rotations in rupture dynamics and ground motion: a case study with implications for the Wenchuan earthquake. *J. Geophys. Res. Solid Earth* 115 (B5). doi:10.1029/2009jb006750

Elsworth, D., Spiers, C. J., and Niemeijer, A. R. (2016). Understanding induced seismicity. *Science* 354 (6318), 1380–1381. doi:10.1126/science.aal2584

Feng, C., Zhang, P., Qi, B., Meng, J., Tan, C., and Hu, D. (2017). The current tectonic stress field of the shallow crust near the Tanlu fault zone. *Mod. Geol.* 31 (01), 46–70. doi:10.3969/j.issn.1000-8527.2017.01.005

Fleitout, L., and Froidevaux, C. (1983). Tectonic stresses in the lithosphere. *Tectonics* 2 (3), 315–324. doi:10.1029/tc002i003p00315

Guo, Q., Wang, C., Ma, H., and Wang, C. (2009). *In-situ* hydro-fracture stress measurement before and after the Wenchuan Ms8.0 earthquake of China. *Chinses J. Geophys.* 52 (05), 1395–2140. (in Chinese with English abstract). doi:10.3969/j.issn.0001-5733.2009.05.029

Guo, R., Zheng, Y., Tian, W., Xu, J., and Zhang, W. (2018). Locking status and earthquake potential hazard along the middle-south Xianshuihe fault. *Remote Sens.* 10 (12), 2048. doi:10.3390/rs10122048

Guo, S., Li, J., Qi, S., Zheng, B., Zhang, T., Waqar, F. M., et al. (2023a). *In-situ* stress data set of Xianshuihe fault zone. *Southwest China*. doi:10.12197/2023GA019

Guo, S., Qi, S., and Cai, M. (2016). Influence of tunnel wall roughness and localized stress concentrations on the initiation of brittle spalling. *Bull. Eng. Geol. Environ.* 75, 1597–1607. doi:10.1007/s10064-015-0816-8

Guo, S., Qi, S., Wang, C., Li, J., Tang, F., and Li, Y. (2023b). *In-situ stress data set of eastern margin of Qinghai-Tibet Plateau*. doi:10.12197/2023GA011

Hardebeck, J. L., and Hauksson, E. (1999). Role of fluids in faulting inferred from stress field signatures. *Science* 285 (5425), 236–239. doi:10.1126/science.285.5425.236

Hardebeck, J. L., Nazareth, J. J., and Hauksson, E. (1998). The static stress change triggering model: constraints from two southern California aftershock sequences. *J. Geophys. Res. Solid Earth* 103 (B10), 24427–24437. doi:10.1029/98jb00573

Harland, W. B. (1971). Tectonic transpression in caledonian Spitsbergen. *Geol. Mag.* 108 (1), 27–41. doi:10.1017/s0016756800050937

Hickman, S., and Zoback, M. (2004). Stress orientations and magnitudes in the SAFOD pilot hole. *Geophys. Res. Lett.* 31 (L15S12), 1–4. doi:10.1029/2004gl020043

Hodgkinson, K. M., Stein, R. S., and King, G. (1996). The 1954 Rainbow Mountain-Fairview Peak-Dixie Valley earthquakes: a triggered normal faulting sequence. *J. Geophys. Res. Atmos.* 1012 (B11), 25459–25471. doi:10.1029/96jb01302

Houseman, G., and England, P. (1993). Crustal thickening versus lateral expulsion in the Indian-Asian continental collision. *J. Geophys. Res. Solid Earth* 98 (B7), 12233–12249. doi:10.1029/93jb00443

Hudson, J. A., and Cooling, C. M. (1988). *In situ* rock stresses and their measurement in the U.K.—Part I. The current state of knowledge. *Pergamon* 25 (6), 363–370. doi:10.1016/0148-9062(88)90976-x

Jaeger, J. C., Cook, N. G. W., and Zimmerman, R. (2009). *Fundamentals of rock mechanics*. John Wiley and Sons, 91–94.

Jiang, G., Xu, X., Chen, G., Liu, Y., Fukahata, Y., Wang, H., et al. (2015). Geodetic imaging of potential seismogenic asperities on the Xianshuihe-Anninghe-Zemuhe fault system, southwest China, with a new 3-D viscoelastic interseismic coupling model. *J. Geophys. Res. Solid Earth* 120 (3), 1855–1873. doi:10.1002/2014jb011492

King, G., Stein, R. S., and Jian, L. (1994). Static stress changes and the triggering of earthquakes. *Bull. Seism. Soc. Am.* 78 (3). doi:10.1785/BSSA0840030935

King, R., Shen, F., Clark Burchfiel, B., Royden, L., Wang, E., Chen, Z., et al. (1997). Geodetic measurement of crustal motion in southwest China. *Geology* 25 (2), 179–182. doi:10.1130/0091-7613(1997)025<0179:gmocmi>2.3.co;2

Lei, X., Ran, Y., Li, Y., Li, H., Gao, Y., and Guo, W. (2021). A possible mechanism for reverse cross-basin fault in Ganyanchi asymmetric pull-apart basin along the Haiyuan fault. *Seismol. Geol.* 43 (1), 36–52. (in Chinese with English abstract). doi:10.3969/j.issn.0253-4967.2021.01.003

Li, B., Guo, Q., Jiang, D., Ding, L., Wang, J., Xu, J., et al. (2023). Response of shallow geostress to deep geostress and seismic hazard analysis before and after the Wenchuan and Lushan earthquakes. *Acta Geol. Sin.* 97 (2), 339~348. doi:10.19762/j.cnki.dizhixuebao.2022013

Li, F. Q., Sun, S. Z., and Li, L. Q. (1982). *In-situ* stress measurement in North China and Tanlu fault zones. *J. Rock Mech. Eng.* (01), 73–86. (in Chinese with English abstract).

Li, J., Zhou, B., Li, T., Yang, Y., and Li, Z. (2020). Locking depth, slip rate, and seismicity distribution along the Daofu-Kangding segment of the Xianshuihe fault system, eastern Tibetan Plateau. *J. Asian Earth Sci.* 193, 104328. doi:10.1016/j.jseaes.2020.104328

Li, L., Wu, Y., Li, Y., Zhan, W., and Liu, X. (2022a). Dynamic deformation and fault locking of the Xianshuihe Fault Zone, Southeastern Tibetan Plateau: implications for seismic hazards. *Earth, Planets Space* 74 (1), 35. doi:10.1186/s40623-022-01591-9

Li, P., and Cai, M. (2018). Distribution law of *in situ* stress field and regional stress field assessments in the Jiaodong Peninsula, China. *J. Asian Earth Sci.* 166, 66–79. doi:10.1016/j.jseaes.2018.07.021

Li, X., Hergert, T., Henk, A., and Zeng, Z. (2022b). Contemporary background stress field in the eastern Tibetan Plateau: insights from 3D geomechanical modeling. *Tectonophysics* 822, 229177. doi:10.1016/j.tecto.2021.229177

Li, Y., Liu, M., Li, Y., and Chen, L. (2019). Active crustal deformation in southeastern Tibetan Plateau: the kinematics and dynamics. *Earth Planet. Sci. Lett.* 523, 115708. doi:10.1016/j.epsl.2019.07.010

Li, Y., Liu, M., Wang, Q., and Cui, D. (2018). Present-day crustal deformation and strain transfer in northeastern Tibetan Plateau. *Earth Planet. Sci. Lett.* 487, 179–189. doi:10.1016/j.epsl.2018.01.024

Liao, C., Zhang, C., Wu, M., Ma, Y., and Ou, M. (2003). Stress change near the Kunlun fault before and after the Ms 8.1 Kunlun earthquake. *Geophys. Res. Lett.* 30 (20). doi:10.1029/2003gl018106

Lin, W., Conin, M., Moore, J. C., Chester, F. M., Nakamura, Y., Mori, J. J., et al. (2013). Stress state in the largest displacement area of the 2011 Tohoku-Oki earthquake. *Science* 339 (6120), 687–690. doi:10.1126/science.1229379

Lin, X., Yuan, H., Xu, P., Yang, X., Xu, Z., Sun, H., et al. (2017). Zonational characteristics of earthquake focal mechanism solutions in North China. *Chin. J. Geophys* 60 (12), 4589–4622. (in Chinese with English abstract). doi:10.6038/cjg20171206

Liu, J., Ren, Z., Min, W., Ha, G., and Lei, J. (2021). The advance in obtaining fault slip rate of strike slip fault-A review. *Earthq. Res. Adv.* 1 (4), 100032. doi:10.1016/j.eqrea.2021.100032

Liu, Q., Chen, J., Li, S., Li, Y., Wang, J., Guo, B., et al. (2008). "Wenchuan Ms8. 0 earthquake: the crustal velocity structure and stress field from the western-sichuan seismic array observations," in AGU Fall Meeting Abstracts. 2008. U22B-01.

Liu, Y., Li, H., Pei, Q., Yu, C., Luo, C., and Yang, F. (2011). Study of distribution regularities of *in-situ* stress field in steep and narrow river valleys. *Chin. J. Rock Mech. Eng.* 30 (12), 2435–2443. (in Chinese with English abstract).

Liu, Y., Luo, C., Li, H., and Wang, X. (2005). Study on *in-situ* stress measurements and characteristics of *in-situ* stress field in west route of South-to-North Water Transfer Project. *Chin. J. Rock Mech. Eng.* 24 (20), 3620–3624. (in Chinese with English abstract).

Liu, Z., Wang, C., Xu, X., Shen, N., and Jia, J. (2017). Analysis of the sliding trend of the middle segment of the Tanlu fault zone based on the measured data of *in-situ* stress. *Mod. Geol.* 31 (04), 869–876. doi:10.3969/j.issn.1000-8527.2017.04.021

Lowell, J. D. (1972). Spitsbergen Tertiary orogenic belt and the Spitsbergen fracture zone. *Geol. Soc. Am. Bull.* 83 (10), 3091–3102. doi:10.1130/0016-7606(1972)83[3091:stobat]2.0.co;2

Ma, J., Zhou, B., Wang, M., Guo, P., Liu, J., Ha, G., et al. (2022). Surface rupture and slip distribution along the Zheduotang fault in the kangding section of the Xianshuihe Fault zone. *Lithosphere* 2021 (2), 6500707. doi:10.2113/2022/6500707

Molnar, P., and Tapponnier, P. (1975). Cenozoic Tectonics of Asia: effects of a Continental Collision: features of recent continental tectonics in Asia can be interpreted as results of the India-Eurasia collision. *Science* 189 (4201), 419–426. doi:10.1126/science.189.4201.419

Molnar, P., and Tapponnier, P. (1978). Active tectonics of tibet. *J. Geophys. Res. Solid Earth.* 83 (B11), 5361–5375. doi:10.1029/jb083ib11p05361

Morris, A., Ferrill, D. A., and Henderson, D. B. (1996). Slip-tendency analysis and fault reactivation. *Geology* 24, 275–278. doi:10.1130/0091-7613(1996)024<0275:staafr>2.3.co;2

Oglesby, D. D., and Day, S. M. (2002). Stochastic fault stress: implications for fault dynamics and ground motion. *Bull. Seismol. Soc. Am.* 92 (8), 3006–3021. doi:10.1785/0120010249

Papadimitriou, E., Wen, X., Karakostas, V., and Jin, X. (2004). Earthquake triggering along the Xianshuihe fault zone of western Sichuan, China. *Pure Appl. Geophys.* 161, 1683–1707. doi:10.1007/s00024-003-2471-4

Peltzer, G., and Saucier, F. (1996). Present-day kinematics of Asia derived from geological fault rates. *J. Geophys. Res.* 101 (27), 943–956. doi:10.1029/96JB02698

Peltzer, G., and Tapponnier, P. (1998). Formation and evolution of strike-slip faults, rifts, and basins during the India-Asia collision: an experimental approach. *J. Geophys. Res.* 103 (15), 85–117. doi:10.1029/JB093iB12p15085

Provost, A. S., and Houston, H. (2001). Orientation of the stress field surrounding the creeping section of the San Andreas Fault: evidence for a narrow mechanically weak fault zone. *J. Geophys. Res. Solid Earth* 106 (B6), 11373–11386. doi:10.1029/2001jb900007

Qian, H. (1988). Identification of potential seismic area along the Xianshuihe zone. *Earthquake Research in Sichuan* (2), 22–30. (in Chinese)

Qiao, X., and Zhou, Y. (2021). Geodetic imaging of shallow creep along the Xianshuihe fault and its frictional properties. *Earth Planet. Sci. Lett.* 567, 117001. doi:10.1016/j.epsl.2021.117001

Qin, X., Zhang, P., Feng, C., Sun, W., Tan, C., Chen, Q., et al. (2014). *In-situ* stress measurements and slip stability of major faults in Beijing region, China. *Chin. J. Geophys.* 57 (7), 2165–2180. doi:10.6038/cjg20140712

Qiu, J., Wu, M., Fan, T., Zhang, C., and Wang, L. (2019). Study on the characteristics of stress accumulation and seismic risk in Sulu boundary of Tanlu fault zone. *J. Geol.* 93 (12), 3249–3258. (in Chinese with English abstract). doi:10.3969/j.issn.0001-5717.2017.05.001

Ren, Y., Wang, D., Li, T., Ran, X., Liu, Z., and Zhang, J. (2021). Analysis of *in-situ* stress characteristics and engineering effects of Ya'an-Xindu Bridge section of Sichuan-Tibet Railway. *J. Rock Mech. Eng.* 40 (01), 65–76. (in Chinese with English abstract). doi:10.13722/j.cnki.jrme.2020.0537

Replumaz, A., and Tapponnier, P. (2003). Reconstruction of the deformed collision zone between India and Asia by backward motion of lithospheric blocks. *J. Geophys. Res. Solid Earth* 108 (B6), 2285. doi:10.1029/2001jb000661

Royden, L. H., Burchfiel, B. C., King, R. W., Wang, E., Chen, Z., Shen, F., et al. (1997). Surface deformation and lower crustal flow in eastern Tibet. *Science* 276 (5313), 788–790. doi:10.1126/science.276.5313.788

Royden, L. H., Burchfiel, B. C., and van der Hilst, R. D. (2008). The geological evolution of the Tibetan Plateau. *science* 321(5892): 1054–1058. doi:10.1126/science.1155371

Sanderson, D. J., and Marchini, W. R. D. (1984). Transpression. *J. Struct. Geol.* 6 (5), 449–458. doi:10.1016/0191-8141(84)90058-0

Sbar, M. L., Engelder, T., Plumb, R., and Marshak, S. (1979). Stress pattern near the san Andreas fault, palmdale, California, from near-surface *in situ* measurements. *J. Geophys. Research-Solid Earth* 84 (B1), 156–164. doi:10.1029/jb084ib01p00156

Scholz, C. H. (2000). Evidence for a strong san Andreas fault. *Geology* 28 (2), 163–166. doi:10.1130/0091-7613(2000)028<0163:efassa>2.3.co;2

Shamir, C., and Zoback, M. D. (1992). Stress orientation profile to 3.5 km depth near the san Andreas fault at cajon pass, California. *J. Geophys. Res.* 97 (B4), 5059–5080. doi:10.1029/91jb02959

Shen, Z. K., Lü, J., Wang, M., and Bürgmann, R. (2005). Contemporary crustal deformation around the southeast borderland of the Tibetan Plateau. *J. Geophys. Res. Solid Earth* 110, B11409. doi:10.1029/2004jb003421

Sheng, S., Hu, X., Wang, X., Wan, Y., Li, H., Li, Z., et al. (2022). Research on crustal stress field in Yunnan and its adjacent areas. *Chin. J. Geophys.* 65 (09), 3252–3267. (in Chinese with English abstract). doi:10.6038/cjg2022P0536

Sibson, R. H. (1980). Power dissipation and stress levels on faults in the upper crust. *J. Geophys. Res. Solid Earth* 85 (B11), 6239–6247. doi:10.1029/jb085ib11p06239

Su, S. (2002). Influence of fault structure on *in-situ* stress field and its engineering significance. *Chin. J. Rock Mech. Eng.* (02), 296. (in Chinese with English abstract).

Su, S., Zhu, H., Wang, S., and Stephansson, O. (2003). The influence of rock physical and mechanical properties on the stress field near faults. *Chin. J. Rock Mech. Eng.* (03), 370–377. (in Chinese with English abstract).

Suo, L., Xu, Z., Feng, T., Wang, Z., Yi, X., Lin, Z., et al. (2022). Inversion and analysis of *in-situ* stress in a tunnel in the Xianshuihe structural belt. *J. Southwest Jiaot. Univ.* 57 (02), 331–338. (in Chinese with English abstract). doi:10.3969/j.issn.0258-2724.20210945

Sylvester, A. G. (1988). Strike-slip faults. *Geol. Soc. Am. Bull.* 100 (11), 1666–1703. doi:10.1130/0016-7606(1988)100<1666:ssf>2.3.co;2

Tanaka, Y., Nakajima, T., and Satio, T. (1981). The Crustal stress field in the Japanese Island-A general view of the results of *in-situ* stress measurements. *J. Geod. Soc. Jpn* 26, 322–326.

Tanaka, Y., Fujimori, K., and Otsuka, S. (1998). *In situ* stress measurement and prediction of great earthquake. *Earthquake (in Japanese)* 50 (2), 201–208.

Tapponnier, P., and Molnar, P. (1976). Slip-line field theory and large-scale continental tectonics. *Nature* 264 (5584), 319–324. doi:10.1038/264319a0

Tapponnier, P., and Molnar, P. (1977). Active faulting and tectonics in China. *J. Geophys. Res.* 82 (20), 2905–2930. doi:10.1029/jb082i020p02905

Tapponnier, P., Peltzer, G., Le Dain, A. Y., Armijo, R., and Cobbold, P. (1982). Propagating extrusion tectonics in Asia: new insights from simple experiments with plasticine. *Geology* 10, 611–616. doi:10.1130/0091-7613(1982)10<611:petian>2.0.co;2

Tapponnier, P., Xu, Z., Roger, F., Meyer, B., Arnaud, N., Wittlinger, G., et al. (2001). Oblique stepwise rise and growth of the Tibet Plateau. *Science* 294 (5547), 1671–1677. doi:10.1126/science.105978

Townend, J., and Zoback, M. D. (2000). How faulting keeps the crust strong. *Geology* 28 (5), 399–402. doi:10.1130/0091-7613(2000)028<0399:hfktcs>2.3.co;2

Wang, E., Meng, K., Su, Z., Meng, Q., Chu, J., Chen, Z., et al. (2014). Block rotation: tectonic response of the Sichuan basin to the southeastward growth of the Tibetan Plateau along the Xianshuihe-Xiaojiang fault. *Tectonics* 33 (5), 686–718. doi:10.1002/2013tc003337

Wang, H., Wright, T., and Biggs, J. (2009). Interseismic slip rate of the northwestern xianshuihe fault from insar data. *Geophys. Res. Lett.* 36 (3), 139–145. doi:10.1029/2008gl036560

Wang, M., Li, T., Meng, L., and Tang, H. (2015). Inversion analysis of stress field at intersection of Y-shaped faults in Sichuan. *J. Railw. Sci. Eng.* 12 (05), 1088–1095. (in Chinese with English abstract). doi:10.19713/j.cnki.43-1423/u.2015.05.016

Wang, M., Shen, Z., Gan, W., Liao, H., Li, T., Ren, J., et al. (2008). GPS monitoring of temporal deformation of the Xianshuihe fault. *Earth Sci.* 51 (9), 1259–1266. doi:10.1007/s11430-008-0095-3

Wang, Y., Cui, X., Hu, X., and Xie, F. (2012). Study on the stress state of the upper crust of the Chinese mainland based on *in situ* stress measurement data. *Acta Geophys.* 55 (09), 3016–3027. (in Chinese with English abstract). doi:10.6038/j.issn.0001-5733.2012.09.020

Wen, X., Allen, C. R., Luo, Z., Qian, H., Zhou, Hu., and Huang, W. (1989). Segmentation, geometric characteristics and seismo-tectonic significance of the Xianshuihe Holocene fault zone. *Acta Seismol. Sin.* (04), 362–372. (in Chinese with English abstract).

Wen, X., and Bai, L. (1985). Study on the deformation combination and movement characteristics of the Xianshuihe active fault zone. *China Earthq.* (04), 55–61. (in Chinese with English abstract).

Wen, X. Z., Ma, S., Xu, X., and He, Y. (2008). Historical pattern and behavior of earthquake ruptures along the eastern boundary of the Sichuan-Yunnan faulted-block, southwestern China. *Phys. Earth Planet. Interiors* 168 (1-2), 16–36. doi:10.1016/j.pepi.2008.04.013

Weng, J. Q., Zeng, L. B., Lyu, W., and Liu, Q. (2020). Width of stress disturbed zone near fault and its influencing factors. *J. Geomechanics* 26 (1), 39–47. doi:10.12090/j.issn.1006-6616.2020.26.01.004

Wilcox, R. E., Harding, T. P., and Seely, D. R. (1973). Basic wrench tectonics. *Aapg Bull.* 57 (1), 74–96. doi:10.1306/819a424a-16c5-11d7-8645000102c1865d

Wu, Q., Li, H., Chevalier, M., Mi, G., Li, C., He, X., et al. (2021). Rock characteristics, internal structure and physical-chemical properties of the Qianning section of the Xianshuihe fault zone. *Acta Petrol. Sin.* 37 (10), 3204–3224. (in Chinese with English abstract). doi:10.18654/1000-0569/2021.10.14

Xie, F., Zhu, J., and Shu, S. (1995). Phased study of the Quaternary tectonic stress field in the Xianshuihe fault zone. *Earthq. Geol.* (01), 35–43. (in Chinese with English abstract).

Xu, G., and Kamp, P. J. J. (2000). Tectonics and denudation adjacent to the Xianshuihe fault, eastern Tibetan Plateau: constraints from fission track thermochronology. *J. Geophys. Res. Solid Earth* 105 (19), 19231–19251. doi:10.1029/2000jb900159

Xu, Z., Meng, W., Guo, C., Zhang, P., Zhang, G., Sun, M., et al. (2021). *In-situ* stress measurement and its application in a deep tunnel in Zheduo Mountain, western Sichuan. *Mod. Geol.* 35 (01), 114–125. (in Chinese with English abstract). doi:10.19657/j.geoscience.1000-8527.2021.018

Yale, D. P. (2003). Fault and stress magnitude controls on variations in the orientation of *in situ* stress. *Geol. Soc. Lond. Spec. Publ.* 209 (1), 55–64. doi:10.1144/gsl.sp.2003.209.01.06

Yale, D. P., Rodriguez, J. M., Mercer, T. B., and Blaisdell, D. W. (1994). *In-situ stress orientation and the effects of local structure-Scott Field*. OnePetro: Rock Mechanics in Petroleum Engineering. North Sea.

Yan, B., and Lin, A. (2015). Systematic deflection and offset of the yangtze river drainage system along the strike-slip ganzi-yushu-xianshuihe fault zone, Tibetan plateau. *J. Geodyn.* 87, 13–25. doi:10.1016/j.jog.2015.03.002

Yan, B., and Lin, A. (2017). Holocene activity and paleoseismicity of the selaha fault, southeastern segment of the strike-slip Xianshuihe Fault zone, Tibetan plateau. *Tectonophysics* 694, 302–318. doi:10.1016/j.tecto.2016.11.014

Yang, S., Yao, R., Cui, X., Chen, Q., and Huang, L. (2012). Analysis of measured stress characteristics of China mainland, various active blocks, and north-south seismic belts. *Acta Geophys.* 55 (12), 4207–4217. doi:10.6038/j.issn.0001-5733.2012.12.032

Zhang, G., Ma, H., Wang, H., and Li, L. (2004). Relationship between active blocks and strong earthquakes in Chinese Mainland. *Sci. China (Series D Earth Sci.)* (07), 591–599. doi:10.3969/j.issn.1674-7240.2004.07.001

Zhang, J., Wen, X., Cao, J., Yan, W., Yang, Y., and Su, Q. (2018). Surface creep and slip-behavior segmentation along the northwestern Xianshuihe fault zone of southwestern China determined from decades of fault-crossing short-baseline and short-level surveys. *Tectonophysics* 722, 356–372. doi:10.1016/j.tecto.2017.11.002

Zhang, L., Su, J., Wang, W., Fang, L., and Wu, J. (2022). Deep fault slip characteristics in the Xianshuihe-Anninghe-Daliangshan Fault junction region (eastern Tibet) revealed by repeating micro-earthquakes. *J. Asian Earth Sci.* 227, 105115–115. doi:10.1016/j.jseaes.2022.105115

Zhang, N., Lan, H., Li, L., Sun, W., Liu, S., Lin, G., et al. (2022). Characteristics and significance analysis of *in-situ* stress measured in the southeast margin of the qinghai-tibet plateau. *Chin. J. Eng. Geol.* 30 (03), 696–707. (in Chinese with English abstract). doi:10.13544/j.cnki.jeg.2022-0112

Zhang, P. Z. (2013). A review on active tectonics and deep crustal processes of the western Sichuan region, eastern margin of the Tibetan Plateau. *Tectonophysics* 584, 7–22. doi:10.1016/j.tecto.2012.02.021

Zhang, P. Z., Li, C. Y., and Mao, F. Y. (2008). Strath terrace formation and strike-slip faulting. *Seismol. Geol.* 30 (1), 44–57.doi:10.3969/j.issn.0253-4967.2008.01.004

Zhang, P. Z., Shen, Z., Wang, M., Gan, W., Burgmann, R., Molnar, P., et al. (2004). Continuous deformation of the Tibetan Plateau from global positioning system data. *Geology* 32 (9), 809–812. doi:10.1130/g20554.1

Zhang, Q. W., Zhang, P. Z., Wang, C., Wang, Y. P., and Ellis, M. A. (2003). Earthquake triggering and delaying caused by fault interaction on Xianshuihe fault belt, southwestern China. *Earthq. Sci.* 16 (2), 156–165. doi:10.1007/s11589-003-0018-5

Zhang, Y. S., Yao, X., Yu, K., Du, G., and Guo, C. (2016). Late-Quaternary slip rate and seismic activity of the Xianshuihe fault zone in southwest China. *Acta Geol. Sinica-English Ed.* 90 (2), 525–536. doi:10.1111/1755-6724.12688

Zhao, X. G., Wang, J., Cai, M., Ma, L., Zong, Z., Wang, X., et al. (2013). *In-situ* stress measurements and regional stress field assessment of the Beishan area, China. *Eng. Geol.* 163, 26–40. doi:10.1016/j.enggeo.2013.05.020

Zheng, G., Wang, H., Wright, T. J., Lou, Y., Zhang, R., Zhang, W., et al. (2017). Crustal deformation in the India-Eurasia collision zone from 25 years of GPS measurements. *J. Geophys. Res. Solid Earth* 122 (11), 9290–9312. doi:10.1002/2017jb014465

Zhou, H., Liu, H. L., and Kanamori, H. (1983). Source processes of large earthquakes along the Xianshuihe fault in southwestern China. *Bull. Seismol. Soc. Am.* 73 (2), 537–551. doi:10.1785/bssa0730020537

Zoback, M. D. (1980). Stress measurements at depth in the vicinity of the San Andreas Fault: implications for the magnitude of shear stress at depth. *J. Geophys. Res. Solid Earth* 85 (B11), 6157–6173. doi:10.1029/jb085ib11p06157

Zoback, M. D. (1992). First-and second-order patterns of stress in the lithosphere: the world stress map Project. *J. Geophys. Res. Solid Earth* 97 (B8), 11703–11728. doi:10.1029/92jb00132

Zoback, M. D., Townend, J., and Grollimund, B. (2002). Steady-state failure equilibrium and deformation of intraplate lithosphere. *Int. Geol. Rev.* 44 (5), 383–401. doi:10.2747/0020-6814.44.5.383